Title: Live cell imaging by 3-imino-(2-phenol)-1,8-naphthalimides : the effect of ex vivo hydrolysis

Author: Mateusz Korzec, Katarzyna Malarz, Anna Mrozek-Wilczkiewicz, Roksana Rzycka-Korzec, Ewa Schab-Balcerzak, Jarosław Polański

Citation style: Korzec Mateusz, Malarz Katarzyna, Mrozek-Wilczkiewicz Anna, Rzycka-Korzec Roksana, Schab-Balcerzak Ewa, Polański Jarosław. (2020). Live cell imaging by 3-imino-(2-phenol)-1,8-naphthalimides : the effect of ex vivo hydrolysis. "Spectrochimica Acta Part A: Molecular and Biomolecular Spectroscopy" Vol. 238 (2020), art. no. 118442, s. 1-12, doi 10.1016/j.saa.2020.118442

Spectrochimica Acta Part A: Molecular and Biomolecular Spectroscopy 238 (2020) 118442

Contents lists available at ScienceDirect

Spectrochimica Acta Part A: Molecular and Biomolecular Spectroscopy

journal homepage: www.elsevier.com/locate/saa

Live cell imaging by 3-imino-(2-phenol)-1,8-naphthalimides: The effect of ex vivo hydrolysis

Mateusz Korzec [a,*], Katarzyna Malarz [b,c], Anna Mrozek-Wilczkiewicz [b,c], Roksana Rzycka-Korzec [a,c], Ewa Schab-Balcerzak [a], Jarosław Polański [a,c]

[a] Institute of Chemistry, University of Silesia in Katowice, 9 Szkolna Str., 40-006 Katowice, Poland
[b] A. Chelkowski Institute of Physics, University of Silesia in Katowice, 75 Pułku Piechoty 1, 41-500 Chorzow, Poland
[c] Silesian Center for Education and Interdisciplinary Research, University of Silesia in Katowice, 75 Pułku Piechoty 1A, 41-500 Chorzow, Poland

ARTICLE INFO

Article history:
Received 17 February 2020
Received in revised form 28 April 2020
Accepted 3 May 2020
Available online 06 May 2020

Keywords:
Live cell imaging
1,8-Naphthalimides
Hydrolysis of imines

ABSTRACT

A series of 3-amino-N-substituted-1,8-naphthalimides and their salicylic Schiff base derivatives were synthesized. The structure of the obtained compounds was confirmed using ^{1}H and ^{13}C NMR, FT-IR spectroscopy and elemental analysis and COSY and HMQC for the representative molecules. The photophysical (UV–Vis, PL) and biological properties of all of the prepared compounds were studied. It was found that the amine with the n-hexyl group in EtOH had the highest PL quantum yield ($\Phi = 85\%$) compared to the others. Moreover, the chelating properties of the azomethines with the n-hexyl group (1a, 1b, 1c) were tested against various cations (Al^{3+}, Ba^{2+}, Co^{2+}, Cu^{2+}, Cr^{3+}, Fe^{2+}, Fe^{3+}, Mn^{2+}, Ni^{2+}, Pb^{2+}, Sr^{2+} and Zn^{2+}) in an acetonitrile, acetone and PBS/AC mixture. Compounds that contained the electron *withdrawing groups* (-Br, -I) had the ability to chelate most of the studied cations, while the unsubstituted derivative chelated only the trivalent cations such as Al^{3+}, Cr^{3+} and Fe^{3+} in acetonitrile. The effect of the environment on the keto-enol tautomeric equilibrium was also demonstrated, especially in the case of the derivative with a bromine atom. The biological studies showed that the tested molecules had no cytotoxicity. Additionally, the ability to image intracellular organelles such as the mitochondria and endoplasmic reticulum was revealed. The crucial role of the hydrolysis of imines for cellular imaging was presented.

1. Introduction

Compounds based on 1,8-naphthalimide unit have an extraordinary thermal and chemical stability and beneficial photophysical properties with high fluorescence quantum yields as well as a biological activity. Therefore, they are widely investigated inter alia as optoelectronic materials, fluorescent sensors or compounds for bioimaging [1]. There are many reports concerning fluorescent sensors that are based on 4-substituted-1,8-naphthalimide [2], which have been successfully used in cell imaging. These reports relate mainly using the sensor for detecting Zn^{2+} [3–6], Cu^{2+} [7], Cu^{+} [8], Hg^{2+} [9], trivalent cations (Al^{3+}, Fe^{3+}, Cr^{3+}) [10] and intracellular compounds, e.g. flufenamic acid [11] or glycosidase [12]. The use of metal complexes that are based on 1,8-naphthalimide in cell imaging such as the Re(I) complex [13] has also been described. Nevertheless, there are only a few literature reports devoted to the sensors based on 3-substituted-1,8-naptalimides [14,15]. On the other hand, the literature has shown the biological activity of compounds that are based on a 1,8-naphthalimide unit substituted in the 3- or 4- position [1,2,16–19]. Using sensors for mitochondrial imaging mainly concerns a detecting reactive oxygen species (ROS), nitric oxide, reactive sulfur species (RSS), thioredoxin (Trx), metal ions and anions [20,21] as well as for detection of viscosity changes [22,23]. Moreover, the aggregation-induced emission luminogens (AIEgens) are used to bioimage various organelles or other important intracellular compounds [24–28]. Nevertheless, most organic dyes exhibit aggregation-caused emission quenching (ACQ) [29] but some of the 1,8-naphthalimide derivatives are known as AIEgens [1].

In previous reports, we showed that 3-substituted-1,8-naptalimides with imine linkages could be efficient materials for organic electronics [30–33]. In addition, we reported the synthesis and use of quinoline derivatives that also contained an imine bond in cell imaging [34,35]. The aim of this work was to investigate a new family of molecules that have 3-substituted-1,8-naptalimide and salicylic imine derivatives as potential agents for cellular imaging. We showed that ketone-enol tautomerism, in which a form of enol-imine is susceptible to hydrolysis, affected the properties of a compound. It was also determined that the keto-imine form was more stable in the cell environment and surprisingly, that it restrained the hydrolysis of a compound.

* Corresponding author.
E-mail address: mateusz.korzec@us.edu.pl (M. Korzec).

https://doi.org/10.1016/j.saa.2020.118442
1386-1425/

2. Experimental section

2.1. Synthesizing the salicylimine 1,8-naphalimide derivatives

The synthesis of the corresponding amines (*stage I and II*, Fig. 1) was carried out according to the procedure described in the previous works [31,33]. The procedure synthesis as well as the characteristics N-substituted 3-amino-1,8-naphalimide derivatives was presented in the supplementary materials (SM). However, below is the procedure for the condensation of amines with salicylic derivatives (*stage III*, Fig. 1) and their structural characteristics.

2.2. General procedure

1 mmol of the corresponding amine (1,2,3), 1 mmol of the salicylaldehyde derivatives (salicylaldehyde, 5-bromosalicylaldehyde, 3,5-dijodosalicylaldehyde), 10 mL of EtOH and three drops trifluoroacetic acid were introduced into the reaction. Next, the vial was closed with a septum. The reaction was carried out for 2 h in an ultrasonic bath, after which the mixture was put into the freezer, and then filtered and washed with ethanol. The product was crystallized from ethyl acetate.

2.2.1. 3-(Imine-(2-hydroxyphenyl))-N-hexyl-1,8-naphthalimide 1a

Yellow solid; Yield = 48%; T_M = 128 °C, *^{1}H NMR* (500 MHz, DMSO) δ 12.71 (s, 1H), 9.23 (s, 1H), 8.53 (d, J = 2.1 Hz, 1H), 8.46 (m, 1H), 8.45 (s, 1H), 8.44 (d, J = 2.1 Hz, 1H), 7.92–7.86 (m, 1H), 7.79 (m, 1H), 7.49–7.45 (m, 1H), 7.04 (m, 2H), 4.07–4.03 (m, 2H), 1.65 (m, 2H), 1.39–1.28 (m, 6H), 0.89–0.82 (m, 3H). *^{13}C NMR* (126 MHz, DMSO) δ 165.59, 163.76, 163.58, 160.77, 147.40, 134.69, 134.38, 133.11, 132.82, 130.69, 128.40, 126.52, 126.07, 124.99, 123.95, 122.62, 119.95, 119.86, 117.21, 31.42, 27.88, 26.64, 22.44, 14.38. *FTIR* (KBr, v, cm^{-1}): 3435 (N-H···O, *hydrogen bonding*), 3139–2992 (C—H aromatic); 2990–2780 (C—H aliphatic); 1698 and 1663 (C=O imide); 1611 (C=C); 1575 (C=C aromatic); 1335 (C—N, aromatic amines). Anal. Calcd for $C_{25}H_{24}N_2O_3$ (400.47 g/mol): C(74.98%) H(6.04%) N(7.00%); found: C(74.67%) H(5.93%) N (7.28%).

2.2.2. 3-(Imine-(5-bromo-2-hydroxyphenyl))-N-hexyl-1,8-naphthalimide 1b

Yellow solid; Yield = 64%; T_M = 150 °C, *^{1}H NMR* (500 MHz, DMSO) δ 12.58 (s, 1H), 9.14 (s, 1H), 8.46 (d, J = 2.1 Hz, 1H), 8.41 (d, J = 0.9 Hz, 1H), 8.40–8.39 (m, 1H), 8.36 (d, J = 2.1 Hz, 1H), 7.95 (d, J = 2.6 Hz, 1H), 7.85 (dd, J = 8.1, 7.4 Hz, 1H), 7.57 (dd, J = 8.8, 2.6 Hz, 1H), 6.97 (d, J = 8.8 Hz, 1H), 4.06–3.99 (m, 2H), 1.63 (m, 2H), 1.38–1.26 (m, 6H), 0.86 (m, 3H). *^{13}C NMR* (126 MHz, DMSO) δ 163.65, 163.58, 163.46, 159.69, 147.13, 136.46, 134.68, 134.24, 132.69, 130.74, 128.37, 126.55, 126.34, 124.64, 123.89, 122.55, 121.89, 119.61, 110.65, 31.41, 27.85, 26.65, 22.44, 14.38. *FTIR* (KBr, v, cm^{-1}): 3435 (N-H···O, *hydrogen bonding*), 3139–2992 (C—H aromatic); 2990–2780 (C—H aliphatic); 1700 and 1661 (C=O imide); 1610 (C=C); 1582 (C=C aromatic); 1332 (C—N, aromatic amines). Anal. Calcd for $C_{25}H_{23}BrN_2O_3$ (479.37 g/mol): C(62.64%) H(4.84%) N(5.84%); found: C(62.55%) H (5.08%) N(5.81%).

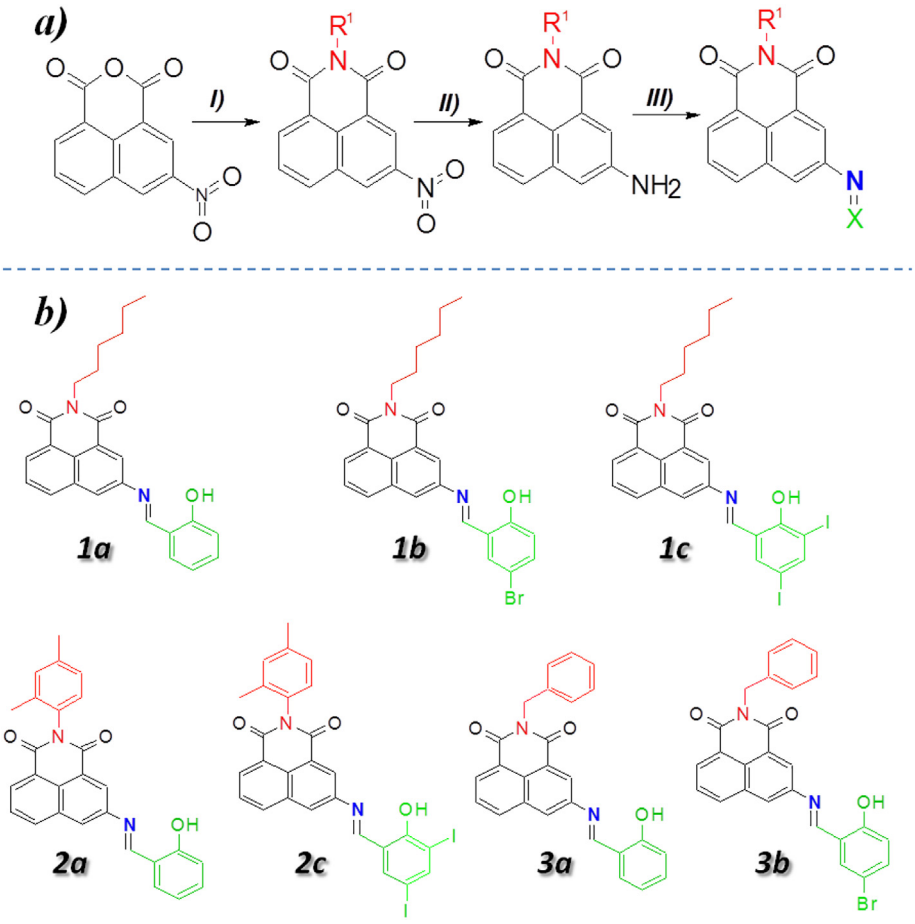

Fig. 1. *a)* Synthesis scheme of naphthalimide derivatives: *(I)* 3-nitro-1,8-naphthalic anhydride, amine (n-hexylamine, 2,4-dimethylaniline, benzylamine), EtOH, 2 h in reflux, *(II)* 10% Pd/C, EtOH, hydrazine, 60 °C, N_2, 6 h, *(III)* EtOH, CF_3COOH, aldehyde (salicylaldehyde, 5-bromosalicylaldehyde, 3,5-diiodosalicylaldehyde) and b) the chemical structures of the final compounds.

2.2.3. 3-(Imine-(3,5-dijodo-2-hydroxyphenyl))-N-hexyl-1,8-naphthalimide 1c

Orange solid; Yield = 53%; T_M = 195 °C, *^{1}H NMR* (400 MHz, $CDCl_3$) δ 14.19 (s, 1H), 8.70 (s, 1H), 8.59 (dd, J = 7.2, 0.9 Hz, 1H), 8.55 (d, J = 2.0 Hz, 1H), 8.22 (d, J = 7.7 Hz, 1H), 8.15 (d, J = 2.0 Hz, 1H), 8.05 (d, J = 1.9 Hz, 1H), 7.84–7.78 (m, 1H), 7.75 (d, J = 2.0 Hz, 1H), 4.18 (m, 2H), 1.73 (m, 2H), 1.47–1.31 (m, 6H), 0.92 (t, J = 7.0 Hz, 3H). *^{13}C NMR* (101 MHz, $CDCl_3$) δ 163.74, 163.55, 161.74, 160.07, 149.88, 145.27, 140.96, 133.82, 132.44, 131.25, 128.04, 127.15, 126.17, 124.51, 123.45, 122.90, 120.43, 87.30, 80.43, 40.70, 31.54, 28.06, 26.78, 22.57, 14.06. *FTIR* (KBr, v, cm^{-1}): 3448 (N-H···O, *hydrogen bonding*), 3139–2992 (C—H aromatic); 2990–2780 (C—H aliphatic); 1699 and 1657 (C═O imide); 1600 (C=C); 1578 (C═C aromatic); 1332 (C—N, aromatic amines). Anal. Calcd for $C_{25}H_{22}I_2N_2O_3$ (652.26 g/mol): C(46.03%) H(3.40%) N(4.29%); found: C(45.93%) H(3.32%) N(4.07%).

2.2.4. 3-(Imine-(2-hydroxyphenyl))-N-2,4-dimetylophenyl-1,8-naphthalimide 2a

Yellow solid; Yield = 76%; T_M = 270 °C, *^{1}H NMR* (400 MHz, DMSO) δ 12.71 (s, 1H), 9.26 (s, 1H), 8.58 (d, J = 1.7 Hz, 1H), 8.53 (m, 2H), 8.49 (d, J = 7.2 Hz, 1H), 7.95 (t, J = 7.8 Hz, 1H), 7.80 (d, J = 6.8 Hz, 1H), 7.48 (t, J = 7.8 Hz, 1H), 7.22 (m, 2H), 7.15 (d, J = 8.1 Hz, 1H), 7.04 (m, 2H), 2.38 (s, 3H), 2.05 (s, 3H). *^{13}C NMR* (101 MHz, DMSO) δ 165.73, 163.74, 163.54, 160.76, 147.56, 138.34, 135.73, 135.00, 134.41, 133.12, 133.05, 132.92, 131.52, 130.92, 129.31, 128.48, 127.73, 127.10, 126.37, 125.21, 124.29, 122.94, 119.98, 119.87, 117.22, 21.18, 17.49. *FTIR* (KBr, v, cm^{-1}): 3440 (N-H···O, *hydrogen bonding*), 3139–2992 (C—H aromatic); 2990–2780 (C—H aliphatic); 1703 and 1668 (C═O imide); 1611 (C=C); 1574 (C═C aromatic); 1337 (C—N, aromatic amines). Anal. Calcd for $C_{27}H_{20}N_2O_3$ (420.46 g/mol): C(77.13%) H(4.79%) N(6.66%); found: C(77.03%) H(4.87%) N(6.71%).

2.2.5. 3-(Imine-(3,5-dijodo-2-hydroxyphenyl))-N-2,4-dimetylophenyl-1,8-naphthalimide 2c

Yellow solid; Yield = 59%; T_M = 215 °C, *^{1}H NMR* (400 MHz, $CDCl_3$) δ 14.22 (s, 1H), 8.74 (s, 1H), 8.66 (d, J = 6.9 Hz, 1H), 8.63 (d, J = 2.0 Hz, 1H), 8.32 (d, J = 8.1 Hz, 1H), 8.17 (dd, J = 10.7, 1.9 Hz, 2H), 7.87 (t, J = 7.8 Hz, 1H), 7.77 (d, J = 1.7 Hz, 1H), 7.24 (s, 1H), 7.19 (d, J = 8.1 Hz, 1H), 7.11 (d, J = 7.9 Hz, 1H), 2.42 (s, 3H), 2.16 (s, 3H). *^{13}C NMR* (101 MHz, $CDCl_3$) δ 163.66, 163.45, 162.07, 160.11, 149.95, 145.51, 141.05, 139.10, 135.37, 134.23, 132.70, 131.94, 131.72, 131.70, 128.17, 128.12, 127.93, 127.69, 126.55, 124.65, 123.98, 123.01, 120.47, 87.28, 80.42, 21.25, 17.56. *FTIR* (KBr, v, cm^{-1}): 3440 (N-H···O, *hydrogen bonding*), 3139–2992 (C—H aromatic); 2990–2780 (C—H aliphatic); 1669 and 1656 (C═O imide); 1613 (C=C); 1571 (C═C aromatic); 1333 (C—N, aromatic amines). Anal. Calcd for $C_{27}H_{18}I_2N_2O_3$ (672.25 g/mol): C(48.24%) H(2.70%) N(4.17%); found: C(48.15%) H(2.84%) N(3.98%).

2.2.6. 3-(Imine-(2-hydroxyphenyl))-N-benzyl-1,8-naphthalimide 3a

Yellow solid; Yield = 77%; T_M = 217 °C, *^{1}H NMR* (400 MHz, DMSO) δ 12.70 (s, 1H), 9.23 (s, 1H), 8.57 (s, 1H), 8.52–8.45 (m, 3H), 7.90 (t, J = 7.4 Hz, 1H), 7.78 (d, J = 7.8 Hz, 1H), 7.48 (t, J = 7.8 Hz, 1H), 7.38 (s, 2H), 7.32 (t, J = 7.4 Hz, 2H), 7.25 (m, 1H), 7.03 (m, 2H), 5.28 (s, 2H). ^{13}C NMR (101 MHz, DMSO) δ 165.68, 163.86, 163.71, 160.76, 147.50, 137.76, 134.97, 134.40, 133.10, 132.89, 130.97, 128.86, 128.47, 128.03, 127.86, 127.57, 126.63, 126.35, 125.28, 123.83, 122.50, 119.95, 119.87, 117.21, 43.48. *FTIR* (KBr, v, cm^{-1}): 3435 (N-H···O, *hydrogen bonding*), 3139–2992 (C—H aromatic); 2990–2780 (C—H aliphatic); 1703 and 1664 (C═O imide); 1609 (C=C); 1572 (C═C aromatic); 1330 (C—N, aromatic amines). Anal. Calcd for $C_{26}H_{18}N_2O_3$ (406.43 g/mol): C(76.83%) H(4.46%) N (6.89%); found: C(76.94%) H(4.57%) N(6.86%).

2.2.7. 3-(Imine-(5-bromo-2-hydroxyphenyl))-N-benzyl-1,8-naphthalimide 3b

Yellow solid; Yield = 68%; T_M = 263 °C, *^{1}H NMR* (400 MHz, DMSO) δ 12.59 (s, 1H), 9.20 (s, 1H), 8.57 (s, 1H), 8.52–8.45 (m, 3H), 7.99 (s, 1H), 7.92 (t, J = 7.7 Hz, 1H), 7.61 (d, J = 8.8 Hz, 1H), 7.39 (d, J = 7.5 Hz, 2H), 7.32 (t, J = 7.1 Hz, 2H), 7.25 (m, 1H), 7.01 (d, J = 8.8 Hz, 1H), 5.29 (s, 2H). *^{13}C NMR* (101 MHz, DMSO) δ 163.85, 163.80, 163.73, 159.70, 147.43, 137.75, 136.55, 135.02, 134.26, 132.84, 131.09, 128.86, 128.53, 128.02, 127.57, 126.82, 126.69, 125.08, 123.91, 122.56, 122.02, 119.68, 110.71, 43.49. *FTIR* (KBr, v, cm^{-1}): 3440 (N-H···O, *hydrogen bonding*), 3139–2992 (C—H aromatic); 2990–2780 (C—H aliphatic); 1698 and 1662 (C═O imide); 1609 (C=C); 1572 (C═C aromatic); 1330 (C—N, aromatic amines). Anal. Calcd for $C_{26}H_{17}BrN_2O_3$ (485.33 g/mol): C (64.34%) H(3.53%) N(5.77%); found: C(64.28%) H(3.59%) N(5.82%).

2.3. Study of the optical properties

The optical properties were tested in solvents of different polarities. For this purpose, weights (1 mg) of each compound were prepared and dissolved in an appropriate amount of DMSO to obtain solutions with a concentration of 1 mM. Then 0.1 mL of the compound solution was metered into volumetric flasks (10 mL), which were then filled up to the mark with the appropriate solvent. The resulting solutions were mixed and left for 2 h, after which the absorption and emission properties of each solution were measured.

2.4. Testing for chelating properties

The chelating properties were tested in equimolar ligand-metal ratio in various solvents (acetone, acetonitryle and PBS/acetone). Chloride cations such as Al^{3+}, Ba^{2+}, Co^{2+}, Cr^{3+},Cu^{2+}, Fe^{2+}, Fe^{3+}, Mn^{2+}, Ni^{2+}, Pb^{2+}, Sr^{2+} and Zn^{2+} as well as octane cobalt were used in the study. 1 mM salt solutions were prepared before use in the following way: the appropriate weights of salt were transferred quantitatively into a 10 mL volumetric flask, which were then filled up to the mark with distilled water. Next, the compounds were weighed (1 mg) and dissolved in DMSO to obtain a concentration of 1 mM. Then, 0.1 mL of the appropriate cation solution and 0.1 mL of the tested compound solution were added into a 10 mL volumetric flask. The flask was supplemented to the mark with a suitable solvent and mixed. Final concentration of compound as well as metal in prepared sample was 10 μM. The solution was left for 2 h, after which the absorbance and emission was measured.

2.5. Cell culture

The human colon carcinoma cell line HCT 116 was purchased from the American Type Culture Collection. The monolayer culture was grown in 75 cm^2 flasks (Nunc) in Dulbecco's modified Eagle's medium, which was supplemented with 12% heat-inactivated fetal bovine serum and a mixture of standard antibiotics – 1% v/v of streptomycin and penicillin (all of the reagents were purchased from Sigma-Aldrich). The cells were cultured under standard conditions at 37 °C in a humidified atmosphere at 5% CO_2 and passaged every three days. The cells were routinely tested for Mycoplasma contamination using the PCR technique before the experiments were started.

2.6. Cytotoxicity studies

The HCT 116 cells were seeded on 96-well transparent plates (Nunc) at a density of $5 \cdot 10^3$ cells per well and incubated under standard conditions for 24 h. Then, the growth medium was replaced with the medium containing the tested compounds at varying concentrations. Stock solutions of the compounds being investigated were prepared in sterile DMSO. The final concentration of DMSO in the medium did not exceed 0.2%. After a 72-h incubation with the tested compounds, the media solutions were replaced with 100 μL DMEM (without serum

and phenol red) and 20 μL of CellTiter 96® AQueous One Solution reagent – MTS (Promega) and incubated for 1 h at 37 °C. The absorbance of the samples was measured at 490 nm using a Synergy 4 multi-plate reader (BioTek). The results are expressed as the percentage of the control (untreated cells) and were calculated as the inhibitory concentration (IC_{50}) values using GraphPad Prism 7. A compound was tested in triplicate in a single experiment with each experiment being repeated at least three times.

2.7. The cellular staining

The HCT 116 cells were seeded onto coverslips at a density of $2 \cdot 10^4$ cells/slide and incubated at 37 °C for 48 h. Then, the medium was replaced with a solution of the tested amines and azomethines at a concentration of 25 μM and the cells were further incubated for 2 h under standard conditions, after which the cells were washed three times with PBS and mounted with a serum-free medium without phenol red. The results of the cellular staining were observed using Zeiss Axio Observer.Z1 inverted fluorescence microscope equipped with an AxioCam MRm camera.

2.8. Colocalization studies

The colocalization studies with some modifications were performed as described previously in [36]. Briefly, HCT 116 cells were seeded onto coverslips at a density of $2 \cdot 10^4$ cells/slide and incubated at 37 °C for 48 h. Then, the medium was replaced with a solution to which compound 1b (25 μM) was added and the cells were further incubated for 2 h. After incubation, the cells were rinsed with PBS and the staining procedures were performed according to the manufacturer's protocols. In short, a medium (without serum and phenol red) that contained MitoTracker® Orange (100 nM, 30 min incubation, Molecular Probes), ER-Tracker™ Red BODIPY® TR Glibenclamide (1 μM, 30 min incubation, Molecular Probes) or LysoTracker® Red DND-99 (500 nM, 1 h incubation, Molecular Probes) were added. After staining with organelle-specific dyes, the cells were washed three times with PBS, then fixed with 3.7% paraformaldehyde for 10 min and mounted with fluoromount-G (Sigma-Aldrich). The subcellular localization was observed using a Nikon Eclipse Ni-U microscope equipped with a Nikon Digital DS-Fi1-U3 camera. The fluorescence images were analyzed and processed using Image J software 1.41 (Wayne Rasband, National Institutes of Health, Bethesda, MD, USA). The PCC and MOC were calculated using the plugin "JACoP" in the Image J software.

3. Discussion of results

3.1. Synthesizing and characterizing compounds

The amines (1–3) were obtained in a two-step reaction starting with the commercially available 3-nitro-1,8-naphthalic anhydride as shown in Fig. 1 and described in supplementary materials (SM) [31,33]. Then, the obtained amines were condensed with commercially available aldehydes such as salicylaldehyde, 5-bromosalicylaldehyde and 3,5-diiodosalicylaldehyde to produce the imines Fig. 1. ^{1}H NMR, ^{13}C NMR and FT-IR studies and an elemental analysis confirmed the chemical structure and purity of the final compounds. In addition, the COSY and HMQC correlation spectra were determined for 1b. Based on the HMQC spectrum (Fig. S2b), the characteristic shifts that indicate the enol-imine form were observed. They included a signal above 12.5 ppm in the form of a singlet that was uncorrelated with carbon and a proton from the imine bond in the form of a singlet (about 9 ppm) that was correlated with carbon (about 160 ppm). Moreover, the COSY spectrum (Fig. S2a) showed that both protons were actually isolated. The HMQC spectrum revealed an additional carbon signal at 39.34 ppm because the hexylamine was covered by a solvent signal (Fig. S2b). Therefore for derivatives 1a and 1b in the aliphatic part signals for five carbons visible in the 1D spectrum was described.

3.2. Spectroscopic studies

UV–Vis and photoluminescence (PL) were measured in the solvents that had various polarities such as chloroform ($CHCl_3$, $\varepsilon = 4.89$), acetone (AC, $\varepsilon = 20.56$), ethanol (EtOH, $\varepsilon = 24.55$), methanol (MeOH, $\varepsilon = 32.66$) and acetonitrile (ACN, $\varepsilon = 35.94$). The obtained spectroscopic data are listed in Table 1, whereas in Fig. S8, the UV–Vis and PL spectra of all of the compounds are presented. In the electronic absorption spectra of the tested compounds (amines and azomethines), a band that is characteristic of the n-π* transitions in the imide unit at 318–350 nm [30,31] was observed in all of the solvents (Fig. S8). In addition, in the UV–Vis spectra of the 3-amino-1,8-naphthalimides, a band in the range of 350 to 470 nm was observed [36].

The largest changes in the absorption spectra were observed for compounds 1c and 2c, which contained two electron-withdrawing substituents (-I) (Fig. S8). This may be due to the significant influence of these substituents on the change of keto-enol tautomeric equilibrium (Fig. 2) [38], which was not clearly visible in the other compounds.

All of the synthesized compounds were luminescent in the investigated solvents and they emitted light that was the maximum PL band (λ_{em}), which was located in the range of 507–550 nm. The calculated Stokes shift for the amines (3107–5281 cm^{-1}) was smaller than for the azomethines (9804–2354 cm^{-1}). The fluorescence lifetime (τ) and fluorescence quantum yield (Φ) of all of the compounds were estimated in two solvents (CH_3Cl and EtOH) (Table 1, Figs. S8, S9 and S10). Slight differences in the times of PL life were noticeable. The lifetime of all of the molecules in chloroform was about 19–20 ns while it was shorter in ethanol (15–20 ns). By contrast, there were significant differences in the PL quantum yield in both solvents. The highest Φ was determined for 3-amino-N-hexyl-1,8-naphtalimide (*1*). Replacing the hexyl unit (*1*) with a diaminophenyl (*2*) or benzyl (*3*) substituent caused a decrease of Φ in both solvents. The azomethines had significantly lower values of Φ compared to the amines, which was associated with occurrence of the photoinduced electron transfer (PET) [39,40]. The existence of the PET phenomenon was also confirmed by the effect of the addition of the base (triethyloamine – Et_3N) and acid (trifluoroacetic acid – TFA) on the optical properties of the imines in the chloroform solution. This type of effect is associated with the protonation of the imine bond by acid, which inhibits the photoinduced electron transfer process, thereby causing an increase in the emission intensity (Fig. S11).

3.2.1. Chelating properties of the compounds in various solvents

The *chelating* properties of compounds 1a, 1b and 1c of various cations (Al^{3+}, Ba^{2+}, Co^{2+}, Cr^{3+}, Cu^{2+}, Fe^{2+}, Fe^{3+}, Mn^{2+}, Ni^{2+}, Pb^{2+}, Sr^{2+} and Zn^{2+}) were investigated in acetone (AC), acetonitrile (ACN) and PBS/AC solutions (80%, 0.1 M PBS). Imine concentrations that were equal to 10 μm and an equimolar amount of each ion were investigated. The complexing properties of the compounds in acetone are shown in

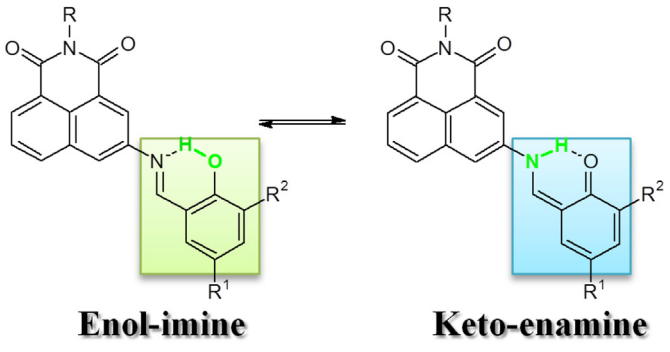

Fig. 2. The enol-ketone tautomeric equilibrium of the 1,8-naphthalimide derivatives.

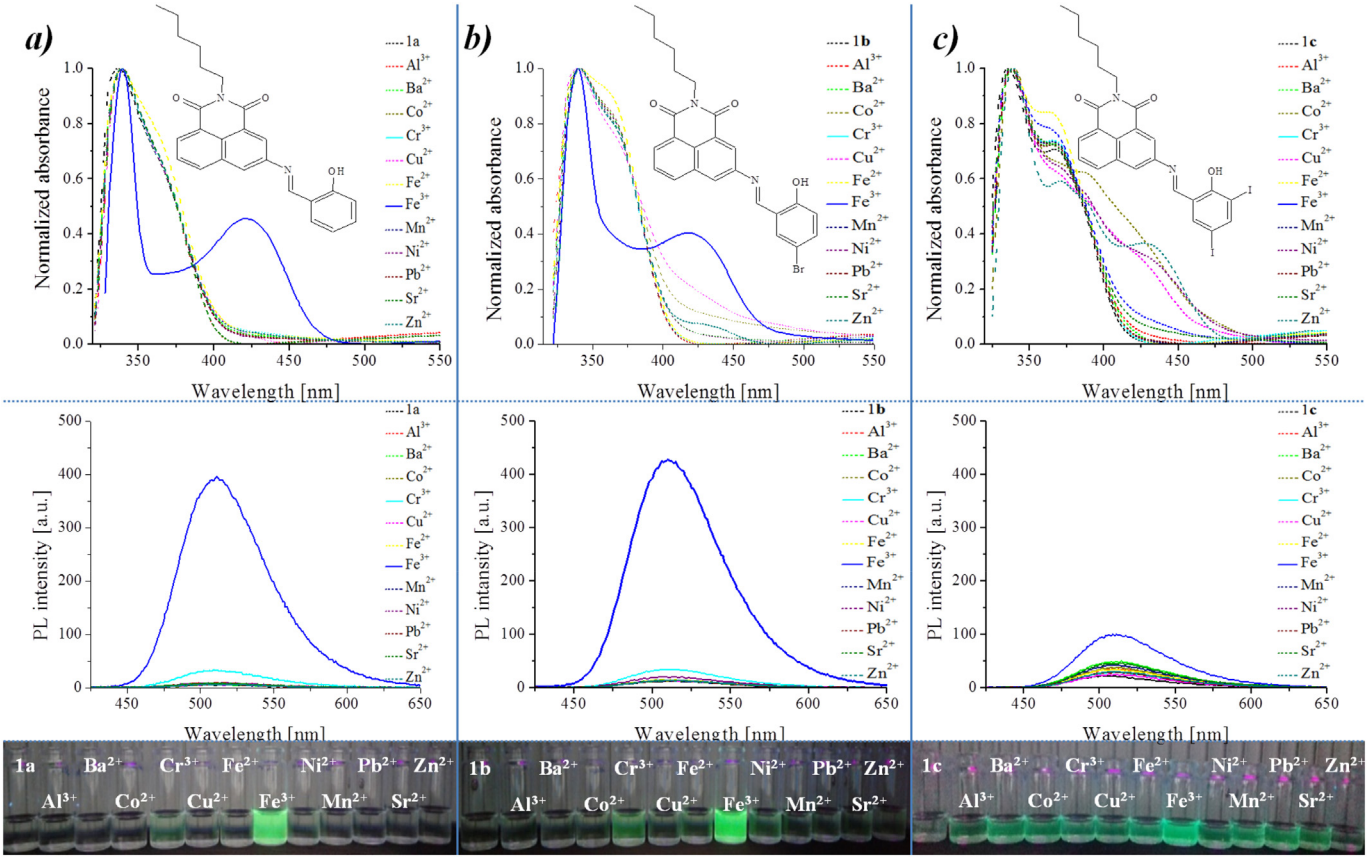

Fig. 3. Changes in the absorption (*upper part of the figure*) and emission (excitation by 340 nm, *lower part of the figure*) relative to the ions (*10 μm*) that were in acetone under identical measuring conditions for the tested compounds (*10 μm*) for a) *1a*, b) *1b*, c) *1c*. On the bottom photos under a UV Lamp at 366 nm were presented.

Fig. 3. In the UV–Vis spectra of complex 1a and 1b with Fe^{3+}, there was a new intense band, which was located at 400–475 nm contrary to 1c. Additionally, for compounds 1a and 1b, there was an increase in the PL intensity in the presence of Fe^{3+} and a slight increase in the emission for the solution with Cr^{3+} There was an increase in the emissions of 1c in the presence of most of the metals, probably due to the predominance of the keto-enamine form [33]. The "turn on" fluorescent properties of all of the compounds were connected with the inhibition of the PET [41–44]. It was found that the complexing properties of the investigated molecules in acetonitrile and acetone were different. In acetonitrile, compound 1a mainly complexed Fe^{3+}, Al^{3+} and Cr^{3+} ions, while compounds 1b and 1c was able to complex most of the cations (Fig. S12).

Thus, in acetonitrile, the keto-enamine form was dominant for 1b and 1c. Next, the metals (Al^{3+}, Cr^{3+} and Fe^{3+}) for a system were titrated with compound 1a in acetonitrile. The emission changes that were the result of the metal titration are presented in Fig. S13. The curves that were plotted showed that the Al^{3+} and Fe^{3+} ions formed a complex more easily compared to the Cr^{3+} ions. In the next stage, the complexing properties in the PBS/AC mixture (80%, 0.1 M PBS) were studied. The changes in the presence of copper ions for all of the compounds are presented (Fig. S14). Fluorescence was extinguished, which may have been associated with the formation of a complex followed by azomethine hydrolysis [45].

3.2.2. Influence of protic solvents on spectroscopic properties

The performed spectroscopic studies in various solvents (Table 1), showed relatively interesting properties of compounds in protic solvents (EtOH, MeOH). First, amines in ethanol had higher quantum yields than analogous imines. Second, the quantum yield in EtOH for imines 1a, 1b, 1c increased with the presence of -B or -I in the compound. The regularities described above reflect very well the collated PL emission spectra and photographs under the UV lamp presented in Fig. S8 in SI. Therefore, it was decided to perform additional studies aimed at explaining the importance of protic solvents (H_2O, EtOH or MeOH) on the spectroscopic properties of compounds. The changes in emissions of aminonaphthalimides due to the intermolecular hydrogen-bonding with protic solvents were proved [37,46,47]. However, the influence of protic solvents on the emission properties of imines is different from that of amines (Table 1, and Fig. S8). Therefore, in the next stage it was decided to perform photophysical tests of compounds (amines and imines) in a binary mixture of solvents (AC/H_2O and EtOH/H_2O) with a different content of water fraction [27,28]. Analysis of such studies will allow obtaining information related to the impact of protic solvent (water) on spectroscopic properties as well as allow studying the photophysical properties of the aggregates formed. First, such tests were performed for both the amines and azomethines in a mixture of acetone with 0.1 M PBS.

The observed changes in emissions because of an increased water content were different for the amines and azomethines. These effects were showed on the superimposed emission spectra (Fig. S15) to determine spectroscopic changes associated with aggregation of compounds. If, as the water content in the system increases, the emission intensity also increases as well as the maximum emission undergoes a bathochromic shift, due to aggregation induced emission (AIE) phenomena. The emission intensity decrease under these conditions, can be caused by the aggregation quenching process [28]. All of the amines (1–3) exhibited aggregation-caused quenching (ACQ), while in the case of imines, there was an increase in emission intensity followed by its quenching. In addition, it was noted that the emission changes for the compounds (1a, 2a, 3a) in the tested system together with the increase of the water content was the same, which means that the substituent in the imide part does not effect on the spectroscopic properties in the

Table 1
The UV–Vis and PL spectroscopic parameters of amines and azomethines.

Medium[a]	Code	UV–Vis	PL				Code	UV–Vis	PL			
		λ_{max} [nm]	λ_{em} [nm]	Stokes shift [cm^{-1}][b]	Φ [%]	τ [ns]		λ_{max} [nm]	λ_{em} [nm]	Stokes shift [cm^{-1}][b]	Φ [%]	τ [ns]
$CHCl_3$	1	340, 407	522	5413	61.43	21.12	1c	318, 373[sh]	528	12,507	3.09	20.91
AC		340, 432	508	3463	–	–		330, 373[sh]	511	10,734	–	–
EtOH		340, 423	546	5326	86.98	17.28		340, 440	546	4997	26.60	17.33
MeOH		340, 428	549	5149	–	–		341, 434	550	4860	–	–
ACN		340, 416	511	4469	–	–		340, 376[sh]	529	10,508	–	–
$CHCl_3$	2	340, 406	520	5400	45.65	20.68	2a	340, 370[sh]	524	10,328	13.65	20.09
AC		340, 438	507	3107	–	–		340, 370[sh]	512	9881	–	–
EtOH		340, 423	545	5292	63.98	17.56		340, 370[sh]	545	11,063	1.39	15.47
MeOH		340, 431	549	4987	–	–		340, 370[sh]	555	11,394	–	–
ACN		340, 417	510	4373	–	–		340, 370[sh]	515	9994	–	–
$CHCl_3$	3	340, 407	522	5413	40.30	19.86	2c	318, 373[sh]	522	12,289	1.62	19.67
AC		340, 423	511	4071	–	–		330, 373[sh]	509	10,657	–	–
EtOH		340, 425	546	5214	34.82	16.96		340, 440	553	4644	5.26	16.84
MeOH		340, 428	553	5281	–	–		341, 434	547	4760	–	–
ACN		340, 417	512	4450	–	–		314, 373[sh]	513	12,354	–	–
$CHCl_3$	1a	340, 373[sh]	520	10,181	13.09	20.78	3a	340, 372[sh]	526	10,400	5.74	20.34
AC		340, 373[sh]	510	9804	–	–		340, 372[sh]	512	9881	–	–
EtOH		340, 373[sh]	548	11,164	2.01	17.03		340, 372[sh]	548	11,164	3.31	20.61
MeOH		340, 373[sh]	552	11,296	–	–		340, 372[sh]	555	11,394	–	–
ACN		340, 373[sh]	510	9804	–	–		340, 372[sh]	514	9957	–	–
$CHCl_3$	1b	340, 370[sh]	523	10,291	5.25	20.79	3b	310, 340, 368[sh]	528	10,472	13.11	21.34
AC		340, 370[sh]	509	9765	–	–		340, 368[sh]	515	9994	–	–
EtOH		310, 340, 370[sh]	547	11,130	21.03	17.52		340, 368[sh]	548	11,164	1.55	17.48
MeOH		310, 340, 370[sh]	550	11,230	–	–		310, 340, 368[sh]	550	11,230	–	–
ACN		310, 340, 370[sh]	510	9804	–	–		310, 340, 368[sh]	515	9994	–	–

[sh] – shoulder.
[a] Dielectric constant of the solvents: $CHCl_3$ (4.89), AC (20.56), EtOH (24.55), MeOH (32.66), ACN (35.94).
[b] The Stokes shifts were calculated according to the equation $\Delta\nu = (1/\lambda_{abs} - 1/\lambda_{em}) \cdot 10^7$ [cm^{-1}].

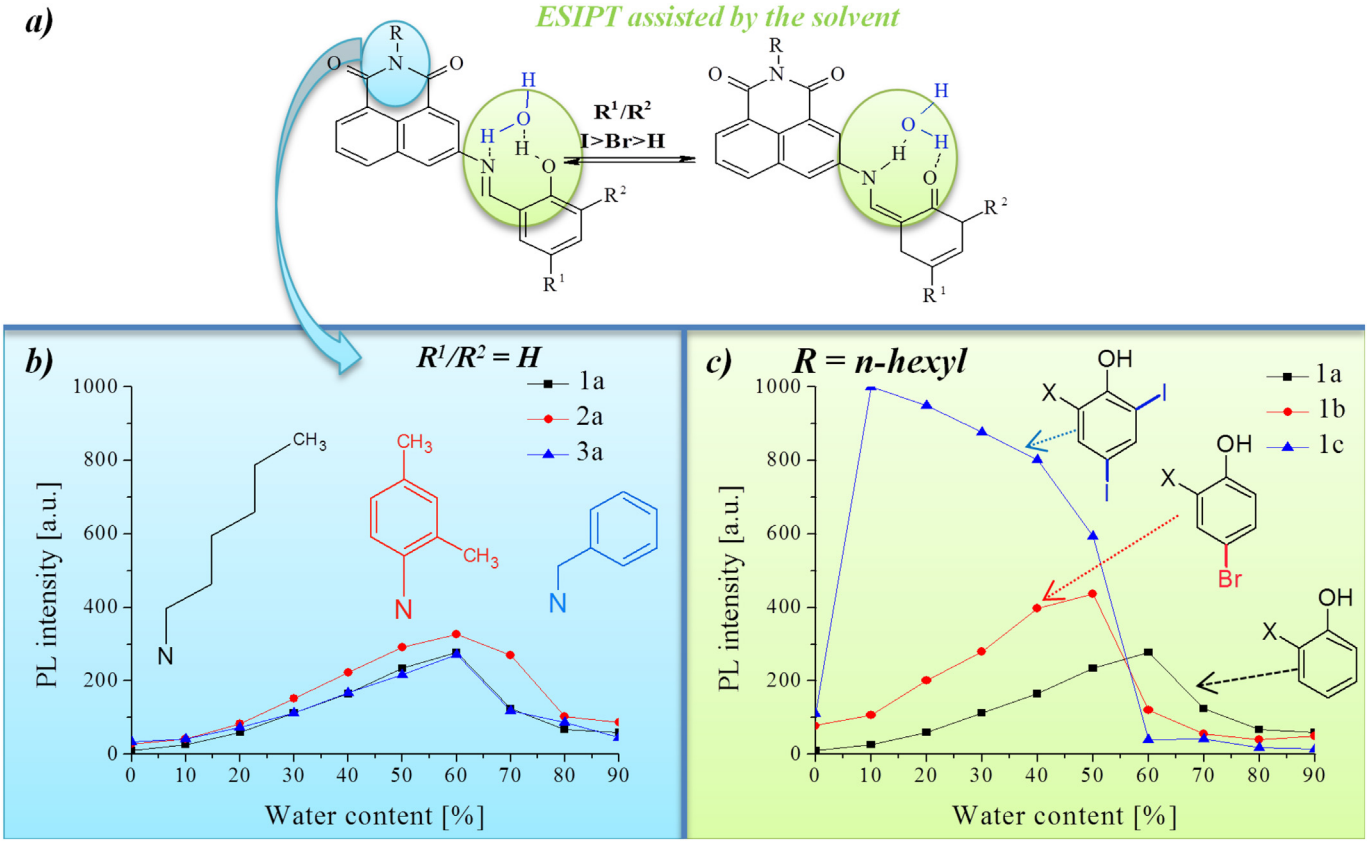

Fig. 4. *a)* The proposed mechanism for the emission increase in the binary acetone-water system; *b)* superimposed graphs of the change in PL intensity because of the increasing water content in the system for 1a, 2a and 3a, *c)* superimposed graphs of the change in emission intensity because of the increasing water content in the system for 1a, 1b and 1c.

presence of a protic solvent (Fig. 4b). Nevertheless, large differences were seen when the substituents in the imine part were changed (Fig. 4c) as was noted for compounds 1a, 1b, 1c. These changes can be explained by the formation of an adduct with water. The electron-withdrawing groups (-Br, -I) stabilize the of the keto-eneamine tautomer by facilitating the solvent-assisted excited or ground state intramolecular proton transfer (ESIPT or GSIPT) – which increase the emission intensity [48,49]. It is visible in the case of the compounds with two iodine atoms (1c and 2c in Fig. S15) in the system with 10% water content. Increasing the water content in the system promotes aggregation of compounds and with water content above 50%, the fluorescence quenching is visible for all compounds. Then, tests were performed in a second system (EtOH/H_2O), which allows checking the complexing properties of compound 1a with respect to iron in ethanol as well as the study of water influence on the forming complex. According to the results presented in Fig. 4, compound 1a does not exhibit such a strong solvent-assisted intramolecular proton transfer as the other analogues. Therefore, it is suitable for these tests in a system with EtOH. In Fig. 5 the changes in emissions caused by the increased water content in the system for the compound itself (Fig. 5a) and the compound with the addition of Fe^{3+} (Fig. 5b) were summarized.

Moreover, the observed changes in the PL intensity depending on the water content in both cases were compiled in Fig. 5c. The addition of iron ions caused an increase in the PL intensity of the system, which indicates also the formation of the complex in such conditions. The obtained results show AIE of both the compound itself and its iron complex. This is demonstrated by the increase in emission intensity and the bathochromic shift in the maximum emission (from 550 to 565 nm) in a system where the water content does not exceed 50%. However, a higher water content in a system reduced the fluorescence intensity in both cases. As was mentioned earlier, the observed PL quenching may have been because of azomethine hydrolysis [50] and/or aggregation-caused quenching (ACQ).

3.3. Biological properties

3.3.1. Cytotoxicity

The promising fluorescent dyes were characterized by a large Stokes shift, which minimized the self-quenching effect and enabled one excitation source to be used with several fluorescence emission channels in order to avoid bleed-through or crosstalk as a result of spectral overlapping. In addition, the strong fluorescence of potential dyes with low photobleaching and pharmacokinetic properties such as protein binding and lipophilicity are decisive for obtaining high-quality images and therefore are valuable in the field of bioimaging application [51]. The most important aspect is the low toxicity of the fluorescent dyes that can be used in biological systems. For this reason, we determined the biological activity of all of the tested amines and azomethines using a colorimetric MTS assay. Considering the potential application of the synthesized compounds in the field of the molecular imaging of cancer, the human colon cancer cell line was used in the tests. The cancer cells were incubated with the tested compounds at various concentrations for 72 h. The results are presented in Table 2.

In general, the substrates – amines did not affect the viability of the cells. A similar behavior was observed for almost all of the tested azomethines, which were inactive at a concentration of 25 μM. The exceptions were 3a and 3b, which were azomethines that were based on the benzylamine moiety, which had a negligible toxic effect on the HCT 116 cells. However, this concentration was acceptable for further microscopic experiments because the tested derivatives reached a strong fluorescence after about a two-hour incubation with the cells.

3.3.2. Cellular imaging

In the next step, we explored the potential of all of the obtained azomethines with their substrates to be fluorescent dyes for bioimaging. These compounds can effectively penetrate the cell membrane after a two-hour incubation, thereby achieving full fluorescence in the cells, which enables them to be visualized using fluorescence microscopy techniques.

The absorption properties of the group of derivatives described above enabled them to be excited using a DAPI or UV-2A filter (excitation 330–380 nm) wavelength. The results are presented as fluorescence images for the azomethine group that was based on the hexylamine moiety in Fig. 6 and in Fig. S16 in the Supporting Materials for the rest of tested derivatives. In general, a very high fluorescence signal was observed for hexylamine (1) and the azomethines with phenol (1a) and 5-bromophenol moieties (1b). The opposite observation was recorded for the 3,5-diiodine derivative (1c) in this group, which was characterized by a very low fluorescence signal in the cells. These results were only partially consistent with the spectroscopic data, in which the highest fluorescence quantum yields were found for hexylamine (87%) and the lowest for compound 1a (2%) in a polar solvent. An explanation for this phenomenon could be the fact that compounds 1a and 1b can probably hydrolyze to hexylamine in biological systems.

The weak fluorescence signal and low quality of the micrographs for the other amines (2, 3) and their corresponding azomethines (2a, 2c and 3a, 3b) was observed. The overall low effect was due to several factors. One reason is that the compounds that were based on the 2,4-dimethylaniline and benzylamine moieties were characterized by low fluorescence quantum yields in both the polar and non-polar solvents. Additionally, the quenching of the fluorescence of iodo-derivatives such as 1c or 2c might have been associated with the high aggregation process, which was caused by a low solubility and a very high lipophilicity (Log P values are presented in Table 2). Moreover, the presence of

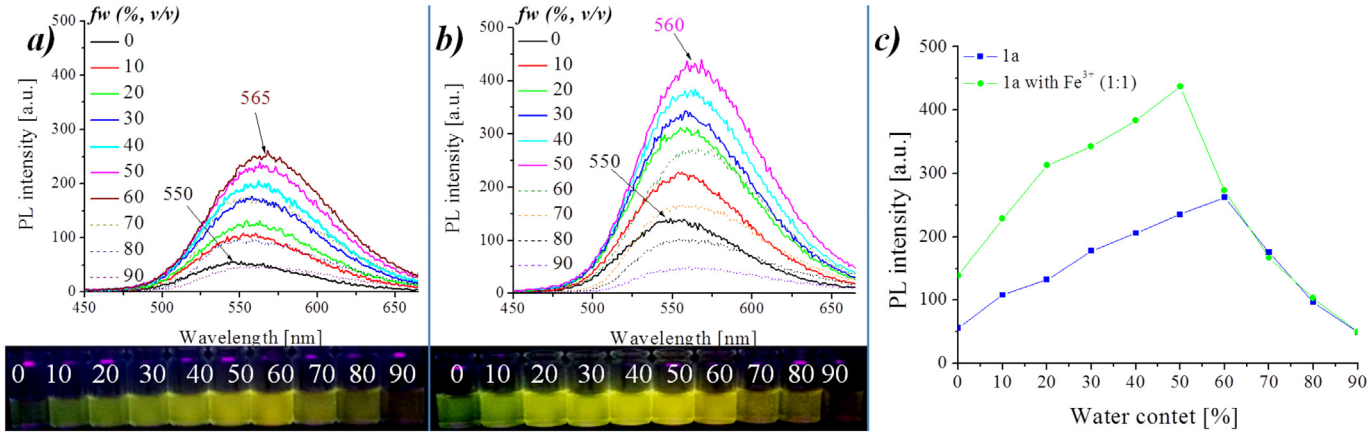

Fig. 5. The photoluminescence (PL) properties of compound 1a (10 μM): (a) in a binary mixture of PBS/EtOH (*fw*: 0,1 M PBS, v/v) with an increasing water (PBS) content (*fw*), (b) after adding of Fe^{3+} (10 μM) to the PBS/EtOH and (c) λ_{em} intensity versus the water content (*fw*) of the solvent mixture with and without Fe^{3+}.

Table 2
Cytotoxicity of the tested compounds against the human colon cancer cell line (HCT 116).

Compounds	IC_{50} [μM]	Log P
1	>25	2.56 ± 0.85
2	>25	2.58 ± 0.85
3	>25	1.68 ± 0.86
1a	>25	4.72 ± 0.93
1b	>25	5.92 ± 0.97
1c	>25	7.26 ± 1.02
2a	>25	4.73 ± 0.93
2c	>25	7.27 ± 1.02
3a	24.76 ± 2.86	3.84 ± 0.94
3b	23.86 ± 1.03	5.04 ± 0.98

two electron-withdrawing substituents (-I) in the C-3 and C-5-positions, which produced a "heavy atom effect" may have enhanced the probability intersystem crossing, which affected the quenching of the fluorescence and this type of behavior in a biological system [52,53]. The preliminary observations suggested that the azomethine derivatives had a tendency to accumulate in the membrane-bound organelles. To evaluate this hypothesis, we determined the subcellular localization of the tested compounds in the human colon cancer cells. The colocalization experiments were performed using the commercially available specific trackers for staining mitochondria (MitoTracker), lysosomes (LysoTracker) and endoplasmic reticulum (ERTracker). For this study, 1b derivative was selected because it had one of the highest fluorescence quantum yields and strong fluorescence signal in living cells of all of the tested derivatives. As is presented in Fig. 7, compound 1b had a tendency to penetrate the mitochondria and endoplasmic reticulum. To confirm the visual data, a quantitative assessment was performed and the Pearson correlation coefficient (PCC) and Mander's overlap coefficient (MOC) were calculated for all of the merged images using ImageJ software [54]. The calculated PCC and MOC for colocalization of the mitochondria were 0.91 and 0.87, respectively. Similar values of 0.94 for the PCC and 0.95 for the MOC were calculated for the overlapping images of the ER and azomethine. These high values confirmed the very strong degree of the accumulation of compound 1b in these organelles [55]. Due to its more lipophilic character, compound 1b may have a stronger tendency to accumulate in the ER structure, which is also in agreement with the literature data [56]. Another possible explanation for azomethines targeting mitochondria-ER is the close contact between these organelles, which form an organized structural and functional network that is mediated by the mitochondrial proteins and mitochondria-related membranes (MAMs) [57]. On the other hand, 1b derivative had a poor affinity to lysosomes (both correlation coefficients were less than 0.4), which indicates that weak bases such as azomethines are not able to effectively diffuse through the lysosomal bilayer and enter the acidic compartments.

3.4. Effect of the keto-enol equilibrium on the hydrolysis of imines

Increased fluorescence after chelating of trivalent metals (Al^{3+}, Fe^{3+} or Cr^{3+}) by naphthalimide derivatives indicates the mechanism of PET inhibition [10,58–60]. Nevertheless, both amines and azomethines were used for cell imaging. Especially derivatives with substituted n-hexyl were very effective. Therefore, another mechanism, e.g. associated with naphthalimide hydrolysis, is more appropriate [50]. It follows that more important, than the complexing properties of imines, is the reported occurrence of imine hydrolysis [33,36,45]. Cell imaging by formation of a complex with metal (PET inhibition) is not excluded, which can explain the brighter points in the Fig. 6 for compound 1a and 1b. Nevertheless, in the context of the results presented in this work, it is appropriate to consider the effect of the keto-enol equilibrium on the hydrolysis of imines. It should be emphasized that the ability of the imine to chelating metals in the presence of water increases the degree of hydrolysis. An example could be the reports of the imine receptors first rapidly coordinating with Au^{3+}, and then hydrolyzing to the corresponding products because of the presence of water [50]. The keto-enol tautomeric equilibrium can be influenced by various factors such as the solvent that is used, the temperature or the substituents [61–63]. The UV–Vis spectra that were registered for the various solvents (Fig. S8) showed significant changes in the tautometric equilibrium. The keto-enol equilibrium seemed to be crucial for the imine hydrolysis process, mainly because of the presence of the electron-withdrawing

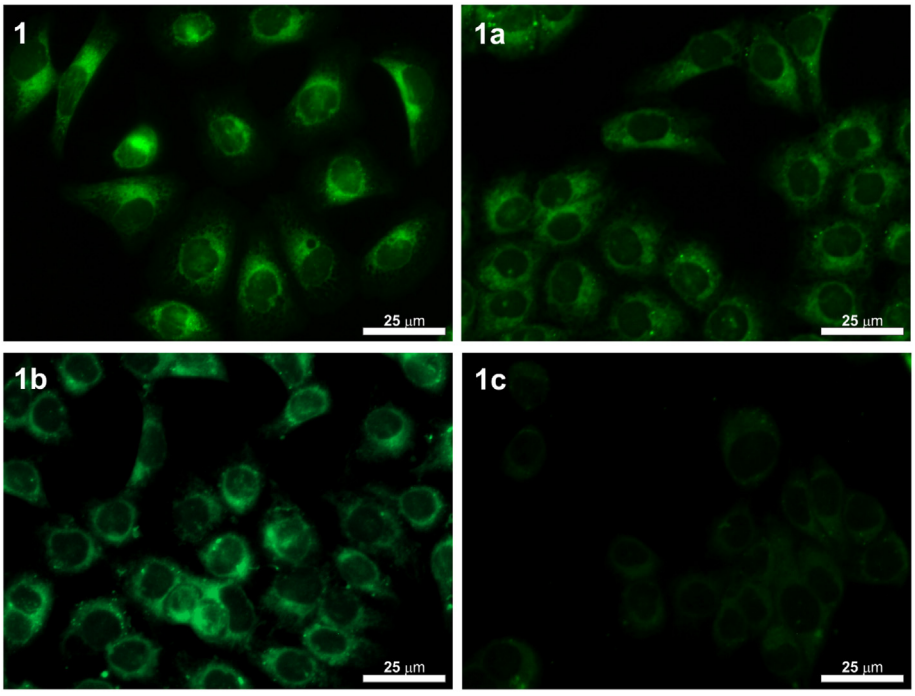

Fig. 6. Fluorescence images of the HCT 116 cells that had been incubated with the compounds at a 25 μM concentration: hexylamine (1) and its corresponding azomethines (1a, 1b, 1c) for 2 h at 37 °C. Scale bars indicate 25 μm.

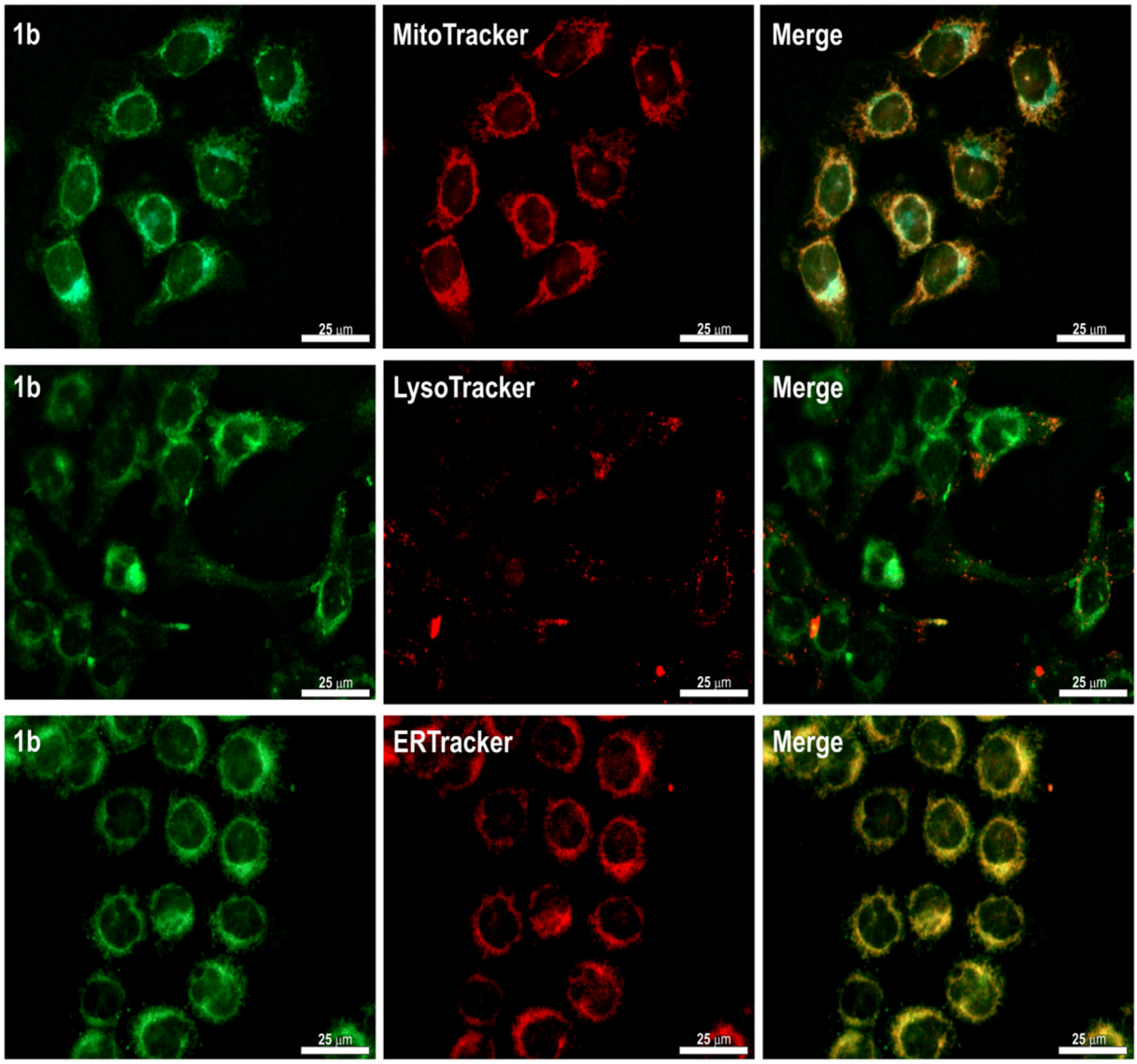

Fig. 7. Fluorescence images of the HCT 116 cells that had been stained with compound 1b, azomethine, (25 μM) and organelle-specific trackers. Panels I and II present the fluorescence of compound 1b or a tracker alone, while panel III presents the merged fluorescence images. Scale bars indicate 25 μm.

substituents. The aggregation properties of stable β-ketoenamines and the hydrolysis of azomethines were discussed in our previous work, where the greater stability of the keto-enamine form in the aquatic environment was demonstrated in our research. These studies showed that the photophysical changes of the imines with an increase of the water content in a system were associated with the hydrolysis process [33]. In these reports, both amines and imines were able to image cell organelles. Amines with the n-hexyl group had the best emission properties in cell imaging. Imines 1a and 1b also imaged the intracellular organelles well, but 1c was not usable. Therefore, the electron-withdrawing groups (-I) shift the equilibrium to ketonimine, which forms a stable adduct with the hydroxyl derivatives or a complex with cations more easily (Fig. 8) as well as not subject to hydrolysis in this form.

Compound 1b may diffuse into the interior of a cell better compared to an amine. At the target location, the environment can affect the keto-enol equilibrium and the enol-imine form can be hydrolyzed to the amine. In turn, compound 1a can be hydrolyzed more easily before entering the cell, and therefore, the result in imaging is comparable to the amine itself. The high impact of the environment on the properties of compound 1b was demonstrated by a change in its complexing properties, i.e. it complexed with two cations in acetone (Fig. 3), while most cations were complexed in acetonitrile (Fig. S12).

4. Conclusions

A series of new N-substituted-1,8-naphthalimide derivatives that have an amine group or imine linkage were prepared. The optical and biological properties of the compounds as well as the ability of selected molecules to complex metal were studied. The synthesized 3-amino-1,8-naphalimides and final naphthalimide-azomethines were photoluminescent in a solution and emitted a green or yellow light. The PL quantum yield was dependent on subtle chemical effects within the tested molecular structure, in particular, imide nitrogen and the aromatic unit substitution pattern of the 1,8-naphthalimide core as well as the solvent type being tested. The naphthalimide-azomethines that had substituted with bromine and iodine atoms had the highest PL Φ of about 20% when tested in in ethanol. The complexing ability of the compounds that were obtained from 3-amino-N-(hexyl)-1,8-naphalimide and salicylaldehyde (1a) and 5-bromosalicylaldehyde

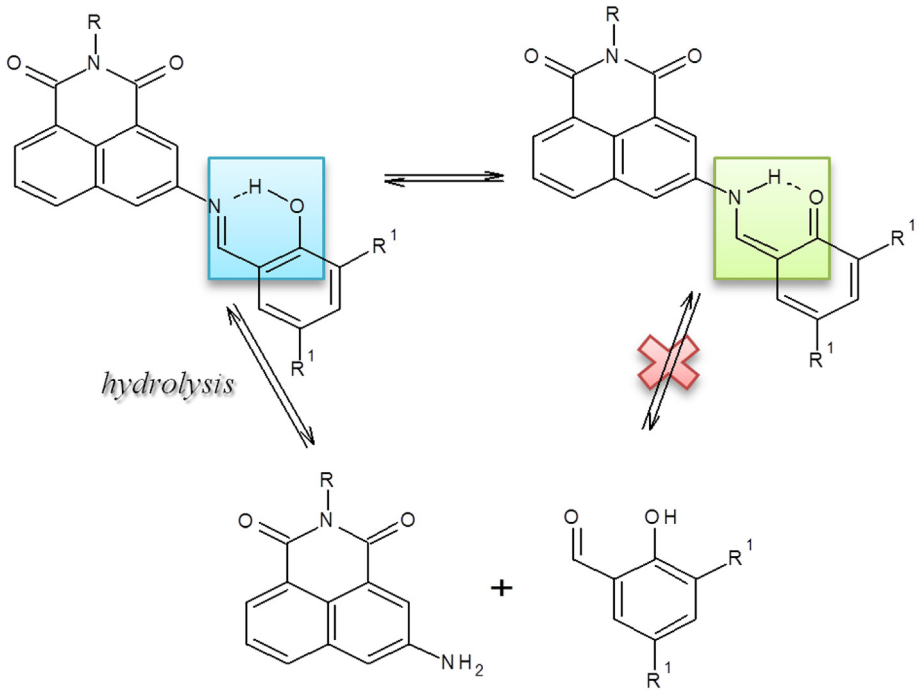

Fig. 8. The proposed mechanism of the influence of the keto-enol equilibrium on the process of the hydrolysis of imines.

(1b) showed a positive potential vs, Fe^{3+} when tested in acetone. The lack of biological activity of the tested series makes these compounds an interesting target as potential cellular imaging dyes. The importance of azomethine to amine hydrolysis, which is responsible for imaging the internal organelles (mitochondria and intraplasmic reticulum) was also demonstrated. The hydrolysis process was affected by the keto-enol equilibrium, while the electron-withdrawing substituents (-I) shifted the equilibrium to keto-enamine. This effect reduced the degree of the hydrolysis. Therefore, compounds 1c and 2c were not efficient in cell imaging. The n-hexyl-naphthalene imide that had been substituted with a bromine atom (1b) or an analogue with an unsubstituted phenyl ring (1a) had the most advantageous cellular imaging behavior.

CRediT authorship contribution statement

Mateusz Korzec: Conceptualization, Methodology, Investigation, Formal analysis, Writing - original draft. **Katarzyna Malarz:** Conceptualization, Methodology, Investigation. **Anna Mrozek-Wilczkiewicz:** Formal analysis, Writing - original draft. **Roksana Rzycka-Korzec:** Investigation. **Ewa Schab-Balcerzak:** Formal analysis, Writing - original draft. **Jarosław Polański:** Writing - original draft.

Declaration of competing interest

The authors declare that they have no known competing financial interests or personal relationships that could have appeared to influence the work reported in this paper.

Acknowledgements

The biological part of these investigations was supported by the National Science Centre 2016/23/N/NZ7/00351 (KM).

Appendix A. Supplementary data

Supplementary data to this article can be found online at https://doi.org/10.1016/j.saa.2020.118442.

References

[1] P. Gopikrishna, N. Meher, P.K. Iyer, Functional 1,8-naphthalimide AIE/AIEEgens: recent advances and prospects, ACS Appl. Mater. Interfaces 10 (2018) 12081–12111, https://doi.org/10.1021/acsami.7b14473.
[2] R.M. Duke, E.B. Veale, F.M. Pfeffer, P.E. Krugerc, T. Gunnlaugsson, Colorimetric and fluorescent anion sensors: an overview of recent developments in the use of 1,8-naphthalimide-based chemosensors, Chem. Soc. Rev. 39 (2010) 3936–3953, https://doi.org/10.1039/B910560N.
[3] J.F. Zhang, S. Kim, J.H. Han, S.J. Lee, T. Pradhan, Q.Y. Cao, S.J. Lee, Ch. Kang, J. Seung Kim, Pyrophosphate-selective fluorescent chemosensor based on 1,8-naphthalimide–DPA–Zn (II) complex and its application for cell imaging, Org. Lett. 19 (2011) 5294–5297, https://doi.org/10.1021/ol202159x.
[4] Ch. Zhang, Z. Liu, Y. Li, W. He, X. Gaod, Z. Guo, In vitro and in vivo imaging application of a 1,8-naphthalimide-derived Zn^{2+} fluorescent sensor with nuclear envelope penetrability, Chem. Commun. 249 (2013) 11430–11432, https://doi.org/10.1039/C3CC46862C.
[5] D. Liua, Y. Zhao, J. Shia, H. Zhu, T. Zhang, P. Qi, J. Chen, F. Yang, H. He, A highly selective and sensitive 1,8-naphthalimide-based fluorescent sensor for Zn^{2+} imaging in living cells, Bioorg. Med. Chem. Lett. 29 (2019) 2646–2649, https://doi.org/10.1016/j.bmcl.2019.07.046.
[6] D. Liu, X. Deng, X. Yin, Y. Wang, J. Guo, J. Chen, G. Yang, H. He, 1,8-Naphthalimide-based fluorescent sensor with high selectivity and sensitivity for Zn^{2+} and its imaging in living cells, Inorg. Chem. Commun. 101 (2019) 117–120, https://doi.org/10.1016/j.inoche.2019.01.023.
[7] G. He, Ch. Liu, X. Liu, Q. Wang, A. Fan, S. Wang, X. Qian, Design and synthesis of a fluorescent probe based on naphthalene anhydride and its detection of copper ions, PLoS One (2017) 1–11, https://doi.org/10.1371/journal.pone.0186994.
[8] C. Satriano, G.T. Sfrazzetto, M.E. Amato, F.P. Ballistreri, A. Copani, M.L. Giuffrida, G. Grasso, A. Pappalardo, E. Rizzarelli, G.A. Tomaselli, R.M. Toscano, A ratiometric naphthalimide sensor for live cell imaging of copper (I), Chem. Commun. 49 (2013) 5565–5567, https://doi.org/10.1039/C3CC42069H.
[9] P.V. Krasteva, M.D. Dimitrova, N.I. Georgiev, V.B. Bojinov, A novel 1,8-naphthalimide probe for selective determination of Hg^{2+} in a wide pH window, J. Chem. Technol. Metall. 53 (2018) 150–158.
[10] F. Ye, N. Wu, P. Li, Y.L. Liu, S.J. Li, Y. Fu, A lysosome-targetable fluorescent probe for imaging trivalent cations Fe^{3+}, Al^{3+} and Cr^{3+} in living cells, Spectrochim. Acta A Mol. Biomol. Spectrosc. 222 (2019) 117242, https://doi.org/10.1016/j.saa.2019.117242.
[11] G. Saito, D. Velluto, M. Resmin, Synthesis of 1,8-naphthalimide-based probes with fluorescent switch triggered by flufenamic acid, R. Soc. Open Sci. 5 (2018) 1–12, https://doi.org/10.1098/rsos.172137.
[12] E. Calatrava-Perez, S.A. Bright, S. Achermann, C. Moylan, M.O. Senge, E.B. Veale, D.C. Williams, T. Gunnlaugsson, E.M. Scanlana, Glycosidase activated release of fluorescent 1,8-naphthalimide probes for tumor cell imaging from glycosylated 'pro-probes', ChemComm 52 (2016) 13086–13089, https://doi.org/10.1039/C6CC06451E.
[13] E.E. Langdon-Jones, C.F. Williams, A.J. Hayes, D. Lloyd, S.J. Coles, P.N. Horton, L.M. Groves, S.J.A. Pope, Luminescent 1,8-naphthalimide-derived ReI complexes:

syntheses, spectroscopy, X-ray structure and preliminary bioimaging in fission yeast cells, Eur. J. Inorg. Chem. (2017) 5279–5287, https://doi.org/10.1002/ejic.201700549.
[14] R.M. Duke, T. Gunnlaugsson, 3-Urea-1,8-naphthalimides are good chemosensors: a highly selective dual colorimetric and fluorescent ICT based anion sensor for fluoride, Tetrahedron Lett. 132 (2011) 1503–1505, https://doi.org/10.1016/j.tetlet.2011.01.099.
[15] J.S. Sidhu, A. Singh, N. Garg, N. Kaur, N. Singh, Gold conjugated carbon dots nano assembly: FRET paired fluorescence probe for cysteine recognition, Sensors Actuators B Chem. 282 (2019) 515–522, https://doi.org/10.1016/j.snb.2018.11.105.
[16] R. Tandon, V. Luxami, H. Kaur, N. Tandon, K. Paul, 1,8-Naphthalimide: a potent DNA intercalator and target for cancer therapy, Chem. Rec. 17 (2017) 956–993, https://doi.org/10.1002/tcr.201600134.
[17] C.L. Fleming, A. Natoli, J. Schreuders, M. Devlin, P. Yoganantharajah, Y. Gibert, K.G. Leslie, E.J. New, T.D. Ashton, F.M. Pfeffer, Highly fluorescent and HDAC6 selective scriptaid analogues, Eur. J. Med. Chem. 162 (2019) 321–333, https://doi.org/10.1016/j.ejmech.2018.11.020.
[18] M.D. Tomczyk, K.Z. Walczak, l,8-Naphthalimide based DNA intercalators and anticancer agents. A systematic review from 2007 to 2017, Eur. J. Med. Chem. 159 (2018) 93–422, https://doi.org/10.1016/j.ejmech.2018.09.055.
[19] W. Ma, S. Zhang, Z. Tia, Z. Xu, Y. Zhang, X. Xia, X. Chen, Z. Liu, Potential anticancer agent for selective damage to mitochondria or lysosomes: naphthalimide-modified fluorescent biomarker half-sandwich iridium(III) and ruthenium(II) complexes, Eur. J. Med. Chem. 181 (2019) 111599, https://doi.org/10.1016/j.ejmech.2019.111599.
[20] Z. Xu, L. Xu, Fluorescent probes for the selective detection of chemical species inside mitochondria, Chem. Commun. 52 (2016) 1094–1119, https://doi.org/10.1039/C5CC09248E.
[21] X. Zhang, Q. Sun, Z. Huang, L. Huang, Y. Xiao, Immobilizable fluorescent probes for monitoring the mitochondria microenvironment: a next step from the classic, J. Mater. Chem. B 7 (2019) 2749–2758, https://doi.org/10.1039/C9TB00043G.
[22] Y. Ma, Y. Zhao, R. Guo, L. Zhua, W. Lin, A near-infrared emission fluorescent probe with multi-rotatable moieties for highly sensitive detection of mitochondrial viscosity in an inflammatory cell model, J. Mater. Chem. B 6 (2018) 6212–6216, https://doi.org/10.1039/C8TB02083C.
[23] H. Li, Ch. Xin, G. Zhang, X. Han, W. Qin, Ch. Zhang, Ch. Yu, S. Jing, L. Li, W. Huang, A mitochondria-targeted two-photon fluorogenic probe for the dual-imaging of viscosity and H_2O_2 levels in Parkinson's disease models, J. Mater. Chem. B 7 (2019) 4243–4251, https://doi.org/10.1039/C9TB00576E.
[24] D. Li, X. Ni, X. Zhang, L. Liu, J. Qu, D. Ding, J. Qian, Aggregation-induced emission luminogen-assisted stimulated emission depletion nanoscopy for superresolution mitochondrial visualization in live cells, Nano Res. 11 (2018) 6023–6033, https://doi.org/10.1007/s12274-018-2118-5.
[25] M. Lin, J. Huang, F. Zeng, S. Wu, A fluorescent probe with aggregation-induced emission for detecting alkaline phosphatase and cell imaging, Chem. Asian J. 14 (2019) 802–808, https://doi.org/10.1002/asia.201801540.
[26] Y. Niu, Y. Qian, Synthesis and aggregation-induced emission enhancement of naphthalimide-rhodamine dye, J. Photochem. Photobiol. A Chem. 329 (2016) 88–95, https://doi.org/10.1016/j.jphotochem.2016.06.020.
[27] Y. Hong, J.W.Y. Lama, B.Z. Tang, Aggregation-induced emission: phenomenon, mechanism and applications, Chem. Commun. 29 (2009) 4332–4353, https://doi.org/10.1039/B904665H.
[28] H. Wang, E. Zhao, Jacky Lam W.Y., B.Z. Tang, AIE luminogens: emission brightened by aggregation, Mater. Today 18 (2015) 365–377, https://doi.org/10.1016/j.mattod.2015.03.004.
[29] Y. Chen, J.W.Y. Lam, R.T.K. Kwok, B. Liu, B.Z. Tang, Aggregation-induced emission: fundamental understanding and future developments, Mater. Horiz. 6 (2019) 428–433, https://doi.org/10.1039/C8MH01331D.
[30] E. Schab-Balcerzak, M. Siwy, M. Filapek, S. Kula, G. Malecki b, K. Laba, M. Lapkowski, H. Janeczek, M. Domanski, New core-substituted with electron-donating group 1,8-naphthalimides towards optoelectronic applications, J. Lumin. 166 (2015) 22–39, https://doi.org/10.1016/j.jlumin.2015.04.025.
[31] S. Kotowicz, M. Korzec, M. Siwy, S. Golba, J.G. Malecki, H. Janeczek, S. Mackowski, K. Bednarczyk, M. Libera, E. Schab-Balcerzak, Novel 1,8-naphthalimides substituted at 3-C position: synthesis and evaluation of thermal, electrochemical and luminescent properties, Dyes Pigments 158 (2018) 65–78, https://doi.org/10.1016/j.dyepig.2018.05.017.
[32] M. Korzec, S. Kotowicz, K. Łaba, M. Łapkowski, J.G. Małecki, K. Smolarek, S. Maćkowski, E. Schab-Balcerzak, Naphthalene diimides prepared by a straightforward method and their characterization for organic electronics, Eur. J. Org. Chem. (15) (2018) 1756–1760, https://doi.org/10.1002/ejoc.201701741.
[33] M. Korzec, S. Kotowicz, R. Rzycka-Korzec, E. Schab-Balcerzak, J.G. Małecki, M. Czichy, M. Łapkowski, Novel β-ketoenamines versus azomethines for organic electronics: characterization of optical and electrochemical properties supported by theoretical studies, J. Mater. Sci. 55 (2020) 3812–3832, https://doi.org/10.1007/s10853-019-04210-3.
[34] W. Cieslik, R. Musiol, M. Korzec, Synthesis of alkyne-substituted quinolines as analogues of allylamines, Int. Bull. Pharm. Sci. 1 (2012) 3–9.
[35] M. Rams-Baron, M. Dulski, A. Mrozek-Wilczkiewicz, M. Korzec, W. Cieslik, E. Spaczyńska, P. Bartczak, A. Ratuszna, J. Polanski, R. Musiol, Synthesis of new styrylquinoline cellular dyes, fluorescent properties, cellular localization and cytotoxic behavior, PLoS One (2015) 1–17, https://doi.org/10.1371/journal.pone.0131210.
[36] B. Czaplińska, K. Malarz, A. Mrozek-Wilczkiewicz, R. Musiol, Acid selective pro-dye for cellular compartments, Sci. Rep. 9 (1) (2019)https://doi.org/10.1038/s41598-019-50734-8.
[37] L. Wang, M. Fujii, M. Yamaji, H. Okamoto, Fluorescence behaviour of 2-, 3- and 4-amino-1,8-naphthalimides: effects of the substitution positions of the amino functionality on the photophysical properties, Photochem. Photobiol. Sci. 17 (2018) 1319–1328, https://doi.org/10.1039/C8PP00302E.
[38] A.M. Asiri, K.O. Badahdah, Synthesis of some new anils: part 1. Reaction of 2-hydroxy-benzaldehyde and 2-hydroxynaphthaldehyde with 2-aminopyridene and 2-aminopyrazine, Molecules 12 (2007) 1796–1804, https://doi.org/10.3390/12081796.
[39] A. Prasanna de Silva, T.S. Moody, G.D. Wright, Fluorescent PET (Photoinduced Electron Transfer) sensors as potent analytical tools, Analyst 134 (2009) 2385–2393, https://doi.org/10.1039/B912527M.
[40] Z.H. Pan, J.W. Zhou, G.G. Luo, Experimental and theoretical study of enol–keto prototropic tautomerism and photophysics of azomethine–BODIPY dyads, Phys. Chem. Chem. Phys. 16 (2014) 16290–16301, https://doi.org/10.1039/C4CP02151G.
[41] X.J. Jiang, H. Tanga, X.Y. Li, S.Q. Zang, H.W. Hou, T.C.W. Mak, Two new isomerous fluorescent chemosensors for Al^{3+} based on photoinduced electron transfer, Spectrochim. Acta A Mol. Biomol. Spectrosc. 115 (2013) 26–32, https://doi.org/10.1016/j.saa.2013.06.006.
[42] W.H. Ding, W. Cao, X.J. Zheng, D.C. Fang, W.T. Wong, L.P. Jin, A highly selective fluorescent chemosensor for AlIII ion and fluorescent species formed in the solution, Inorg. Chem. 52 (2013) 7320–7322, https://doi.org/10.1021/ic401028u.
[43] D. Zhou, Ch. Sun, Ch. Chen, X. Cui, W. Li, Research of a highly selective fluorescent chemosensor for aluminum (III) ions based on photoinduced electron transfer, J. Mol. Struct. 1079 (2015) 315–320, https://doi.org/10.1016/j.molstruc.2014.09.050.
[44] P.A. Panchenko, Y.V. Fedorov, O.A. Fedorova, Selective fluorometric sensing of Hg^{2+} in aqueous solution by the inhibition of PET from dithia-15-crown-5 ether receptor conjugated to 4-amino-1,8-naphthalimide fluorophore, J. Photochem. Photobiol. A Chem. 364 (2018) 124–129, https://doi.org/10.1016/j.jphotochem.2018.06.003.
[45] M. Korzec, S. Senkała, R. Rzycka-Korzec, S. Kotowicz, E. Schab-Balcerzak, J. Polański, A highly selective and sensitive sensor with imine and phenyl-ethynyl-phenyl units for the visual and fluorescent detection of copper in water, J. Photochem. Photobiol. A Chem. 382 (2019) 1118933–1118942, https://doi.org/10.1016/j.jphotochem.2019.111893.
[46] S. Dhar, S.S. Roy, D.K. Rana, S. Bhattacharya, S. Bhattacharya, S.Ch. Bhattacharya, Tunable solvatochromic response of newly synthesized antioxidative naphthalimide derivatives: intramolecular charge transfer associated with hydrogen bonding effect, J. Phys. Chem. A 115 (2011) 2216–2224, https://doi.org/10.1021/jp1117773.
[47] J. Cao, T. Wu, W. Sun, Ch. Hu, Time-dependent density functional theory study on the excited-state hydrogen bonding strengthening of photoexcited 4-amino-1,8-naphthalimide in hydrogen-donating solvents, 26 (2013) 289–294, https://doi.org/10.1002/poc.3084.
[48] B. Das, A. Chakraborty, S. Chakraborty, Experimental and theoretical investigation of ground state intramolecular proton transfer (GSIPT) in salicylideneaniline Schiff base derivatives in polar protic medium, Spectrochim. Acta A Mol. Biomol. Spectrosc. 225 (2020), 117443. https://doi.org/10.1016/j.saa.2019.117443.
[49] N. Alarcos, M. Gutierrez, M. Liras, F. Sanchez, A. Douhal, An abnormally slow proton transfer reaction in a simple HBO derivative due to ultrafast intramolecular-charge transfer events, Phys. Chem. Chem. Phys. 7 (2015) 16257–16269, https://doi.org/10.1039/C5CP00577A.
[50] W. Wang, W. Zhang, Y. Feng, S. Wang, H. Lei, J. Huang, H. Chu, S. Li, X. Wang, Strategically modified highly selective mitochondria-targeted two-photon fluorescent probe for Au^{3+} employing Schiff-base: inhibited C=N isomerization vs. hydrolysis mechanism, Dyes Pigments 150 (2018) 241–251, https://doi.org/10.1016/j.dyepig.2017.12.019.
[51] A. Ettinger, T. Wittmann, Fluorescence live cell imaging, Methods Cell Biol. 123 (2014) 77–94, https://doi.org/10.1016/B978-0-12-420138-5.00005-7.
[52] K.N. Solovyov, E.A. Borisevich, Intramolecular heavy-atom effect in the photophysics of organic molecules, Physics-Uspekhi 48 (2005) 231–253, https://doi.org/10.1070/PU2005v048n03ABEH001761.
[53] J. Sun, A.M.S. Riela, O.B. Berryman, Solvatochromism and fluorescence response of a halogen bonding anion receptor, New J. Chem. 42 (2018) 10489–10492, https://doi.org/10.1039/C8NJ00558C.
[54] S. Bolte, F.P. Cordeliers, A guided tour into subcellular colocalization analysis in light microscopy, J. Microsc. 224 (2006) 213–232, https://doi.org/10.1111/j.1365-2818.2006.01706.x.
[55] V. Zinchuk, Y. Wu, O. Grossenbacher-Zinchuk, Bridging the gap between qualitative and quantitative colocalization results in fluorescence microscopy studies, Sci. Rep. 3 (2013) 1–5, https://doi.org/10.1038/srep01365.
[56] J. Colston, R.W. Horobin, F. Rashid-Doubell, J. Pediani, K.K. Johal, Why fluorescent probes for endoplasmic reticulum are selective: an experimental and QSAR-modelling study, Biotech. Histochem. 78 (2003) 323–332, https://doi.org/10.1080/10520290310001646659.
[57] C. Giorgi, D. De Stefani, A. Bononi, R. Rizzuto, P. Pinton, Structural and functional link between the mitochondrial network and the endoplasmic reticulum, Int. J. Biochem. Cell Biol. 41 (2009) 1817–1827, https://doi.org/10.1016/j.biocel.2009.04.010.
[58] Y. Liu, C. Zhao, X. Zhao, H. Liu, Y. Wang, Y. Du, D. Wei, A selective *N,N*-dithenoyl-rhodamine based fluorescent probe for Fe^{3+} detection in aqueous and living cells, J. Environ. Sci. China 90 (2020) 180–188, https://doi.org/10.1016/j.jes.2019.12.005.
[59] S. Janakipriya, N. Reddy, Ch. Purnasai, K. Sathiah, T. Asit, B. Mandal, Selective interactions of trivalent cations Fe^{3+}, Al^{3+} and Cr^{3+} turn on fluorescence in a naphthalimide based single molecular probe, Spectrochim. Acta A Mol. Biomol. Spectrosc. 153 (2016) 465–470, https://doi.org/10.1016/j.saa.2015.08.044.
[60] T. Anand, A. Kumar, S.K. Sahoo, A new Al^{3+} selective fluorescent turn-on sensor based on hydrazide-naphthalic anhydride conjugate and its application in live cells imaging, Spectrochim. Acta A Mol. Biomol. Spectrosc. 204 (2018) 105–112, https://doi.org/10.1016/j.saa.2018.06.033.

[61] M.A. Rauf, S. Hisaindeea, N. Saleh, Spectroscopic studies of keto–enol tautomeric equilibrium of azo dyes, RSC Adv. 5 (2015) 18097–18110, https://doi.org/10.1039/C4RA16184J.
[62] A. Matwijczuk, D. Karcz, R. Walkowiak, J. Furso, B. Gładyszewska, S. Wybraniec, A. Niewiadomy, G.P. Karwasz, M. Gagos, Effect of solvent polarizability on the keto/enol equilibrium of selected bioactive molecules from the 1,3,4-thiadiazole group with a 2,4-hydroxyphenyl function, J. Phys. Chem. A 121 (2017) 402–1411, https://doi.org/10.1021/acs.jpca.6b08707.
[63] L. Antonov, Tautomerism in azo and azomethyne dyes: when and if theory meets experiment, Molecules 24 (2019) 2252–2265, https://doi.org/10.3390/molecules24122252.